Journal of Power Sources 191 (2009) 407–416

Contents lists available at ScienceDirect

Journal of Power Sources

journal homepage: www.elsevier.com/locate/jpowsour

Developing fuel map to predict the effect of fuel composition on the maximum voltage of solid oxide fuel cells

Siamak Farhad*, Feridun Hamdullahpur

Department of Mechanical & Aerospace Engineering, Carleton University, 1125 Colonel By Drive, Ottawa, ON, Canada K1S 5B6

ARTICLE INFO

Article history:
Received 26 December 2008
Received in revised form 14 February 2009
Accepted 16 February 2009
Available online 9 March 2009

Keywords:
Solid oxide fuel cell
Maximum cell voltage
Fuel map
Ternary coordinate system
Fuel processor
Modeling

ABSTRACT

A thermodynamic model is developed to determine the fuels that would yield an identical maximum cell voltage (MCV) for solid oxide fuel cells (SOFCs) at a given operating condition. These fuels make a continuous curve in the ternary coordinate system. A fuel map is established by developing the continuous fuel curves for different MCVs at the same operating condition and representing them in the carbon–hydrogen–oxygen (C–H–O) ternary diagram. Using the fuel map, the effect of the composition of a fuel containing carbon, hydrogen, oxygen, and inert gas atoms on the MCV of SOFCs can be easily studied. In addition to the effect of the fuel composition, the graphical representation of fuel maps can be applied to study the effect of the fuel processors on the MCV of SOFCs. As a general result, among fuels that can be directly utilized in SOFCs, at the same temperature and pressure, the one located at the intersection of the H–C axis and the carbon deposition boundary (CDB) curve in the C–H–O ternary diagram, provides the highest MCV for SOFCs. The results also show that for the fuels that cannot be directly utilized in SOFC, the steam reforming fuel processor always yields a higher MCV than the autothermal reforming or the partial oxidation fuel processors at the same inlet fuel temperature.

1. Introduction

In addition to the high electrical efficiency, the fuel flexibility is one of the most important advantages of solid oxide fuel cells (SOFCs). Various types of fuels, including hydrogen, carbon monoxide, hydrocarbons, alcohols and biomass can be utilized indirectly or even directly in SOFCs. Usually, a hydrogen- and/or carbon monoxide-rich fuel that does not cause any carbon deposition over the anode catalyst can be directly utilized in SOFCs. The steam reforming [1–3], partial oxidation [4,5], and autothermal reforming [6,7] fuel processors are widely used to prepare fuels that cannot be directly utilized in SOFCs. In addition to these fuel processors, anode exit gas recirculation [8,9] can be applied to prevent carbon deposition over the anode catalyst. Although a broad range of fuels and fuel processors can be used for SOFCs, their effect on the cell performance can vary considerably. In this paper, the effect of the composition of any fuel containing carbon, hydrogen, oxygen, and inert gas atoms on the maximum cell voltage (MCV) of SOFCs is studied.

Since the fuel and oxidant are utilized along the anode and cathode of an SOFC (the partial pressures of fuel and oxidant decrease along the anode and cathode and the partial pressure of products increase along the anode), depending on the cell temperature distribution, the Nernst voltage and internal resistance change at different places of a cell. In most cases, especially at a high fuel utilization ratio, the minimum local Nernst voltage and the maximum local internal resistance take place at the end of the anode (the last point in the anode along the fuel flow channel, where electrochemical reactions take place). In this study, it is assumed that the fuel utilization ratio is sufficiently high so that the minimum local Nernst voltage and the maximum local internal resistance of a cell take place at the end of the anode. At this condition, the MCV of ion-conducting electrolyte SOFCs that operate at a specified anode inlet fuel composition and temperature, anode outlet fuel temperature, cell operating pressure, oxygen mole fraction at the cathode, and fuel utilization ratio, is limited to the minimum local Nernst voltage and can be thermodynamically obtained from the Nernst voltage equation.

Fuel maps are developed to study the effect of the inlet fuel composition on the MCV of SOFCs. For this purpose, a thermodynamic model is developed to identify the fuels that would yield identical MCV for SOFCs at a specified operating condition of anode inlet and outlet fuel temperatures, cell operating pressure, oxygen mole fraction at the cathode, and the fuel utilization ratio. These fuels make a continuous curve in the ternary coordinate system. A fuel map is created by generating the continuous fuel curves for different MCVs at the same operating condition and representing them in the carbon–hydrogen–oxygen (C–H–O) ternary diagram. It is necessary to draw the carbon deposition boundary (CDB) curve in a

* Corresponding author. Tel.: +1 613 520 3806; fax: +1 613 520 2536.
E-mail address: feridun_hamdullahpur@carleton.ca (F. Hamdullahpur).

0378-7753/$ – see front matter © 2009 Elsevier B.V. All rights reserved.
doi:10.1016/j.jpowsour.2009.02.073

Nomenclature

C	carbon atom ratio
$\dot{C}$	consumption rate (mol s^{-1})
F	Faraday constant (=96485 Coulomb mol^{-1})
H	hydrogen atom ratio
$\tilde{g}$	Gibbs free energy (J mol^{-1})
$\tilde{h}$	enthalpy (J mol^{-1})
i	electric current density (A M^{-2})
I	electric current (A)
K_p	equilibrium constant
MCV	maximum cell voltage (V)
$\dot{n}$	molar flow rate (mol s^{-1})
O	oxygen atom ratio
p	pressure (bar)
$\dot{P}$	production rate (mol s^{-1})
R_u	universal gas constant (=8.314 J mol^{-1} K^{-1})
T	temperature (K)
U_f	fuel utilization ratio
$\dot{w}$	electric power (W)
x	mole fraction
y	volumetric mixing ratio
z	ratio of the number of atoms

Greek letters

$\alpha,\beta,\gamma,\delta,\varepsilon,\psi,\omega$	defined parameters
Δ	difference

Subscripts and superscripts

0	standard pressure (=1 bar)
B	Boudouard reaction
CD	carbon decomposition reaction
CDB	carbon deposition boundary
COR	carbon monoxide reduction reaction
i	inlet
ig	inert gas
o	outlet
SR	steam reforming reaction
WGS	water gas shift reaction

fuel map to determine the region of a fuel. The region below the CDB curve belongs to fuels that can be directly utilized in SOFCs. In this paper, this region is called "direct fuel utilization region". The region above the CDB curve belongs to fuels that should be processed before being utilized in SOFCs to prevent carbon deposition over the anode catalyst. In this paper, this region is called "indirect fuel utilization region". After finding the CDB curve, the fuel map can be easily applied to study the effect of the composition of any fuel containing carbon, hydrogen, oxygen and inert gas atoms on the MCV of SOFCs.

2. Model development

At the operating temperatures and pressures of SOFCs, the species of primary importance of the equilibrium products of a fuel, located in the C–H–O ternary diagram, are carbon, C, in solid phase and a mixture of H_2, CO, CH_4, H_2O and CO_2 in the gaseous phase. The species of secondary importance, which are present in minor amounts, are C_2H_6, C_2H_4, and C_2H_2. Species such as CH_3OH, HCHO, C_2H_5OH, and $C_{10}H_{22}$ are present in amounts of several orders of magnitude smaller than the species of secondary importance [10,11]. The chemical species of the equilibrium products of 300 different fuels, located in the C–H–O ternary diagram, including alkanes, alcohols, alkenes, alicyclic hydrocarbons, dimethyl ether, biogas and coke oven gas have also been calculated by Sasaki et al., via the Gibbs free energy minimization method [12]. Their results for the major and minor constituents of equilibrium products of fuels have a good agreement with the results presented in references [10,11].

In the present model, all fuels located in the C–H–O ternary diagram are assumed to be in thermodynamic equilibrium and only the important species of H_2, CO, CH_4, H_2O and CO_2 are taken into account for the gaseous phase of equilibrium products of the fuels. However, inert gases such as nitrogen may be present in this phase. Neglecting the amounts of the minor constituents in the model does not affect the results within the accuracy of the equilibrium constant data [11].

Before presenting the model, the mole fraction of species in the gaseous phase of equilibrium product of a fuel (hereafter called just fuel) is obtained by dividing the partial pressures of H_2, CO, CH_4, H_2O, and CO_2 by the difference of the total gas pressure and the inert gases partial pressure. Using the Dalton's law:

$$x_{H_2} + x_{CO} + x_{CH_4} + x_{H_2O} + x_{CO_2} = 1 \tag{1}$$

The location of a gaseous fuel in the C–H–O ternary diagram can be determined from [11]:

$$C = \frac{x_{CO_2} + x_{CO} + x_{CH_4}}{2x_{H_2} + 3x_{CO_2} + 2x_{CO} + 3x_{H_2O} + 5x_{CH_4}} \tag{2}$$

$$H = \frac{2x_{H_2} + 2x_{H_2O} + 4x_{CH_4}}{2x_{H_2} + 3x_{CO_2} + 2x_{CO} + 3x_{H_2O} + 5x_{CH_4}} \tag{3}$$

$$O = \frac{2x_{CO_2} + x_{CO} + x_{H_2O}}{2x_{H_2} + 3x_{CO_2} + 2x_{CO} + 3x_{H_2O} + 5x_{CH_4}} \tag{4}$$

2.1. Carbon deposition boundary

Depending on the fuel composition, temperature and pressure, the presence of the solid carbon in a gaseous mixture is possible. The solid carbon may form on the anode catalyst and deactivate it for electrochemical reactions [13,14]. As a preliminary step to develop fuel maps, the CDB curve should be determined based on thermodynamic equilibrium or considering the influence of the anode catalyst using a detailed kinetics modeling or experiment. These methods have been studied extensively by researchers [11,12,15–24]. To obtain the CDB curve for fuel maps in this paper, the thermodynamic equilibrium method suggested by Broers et al. [11] was simplified.

In thermodynamic equilibrium, the CDB curve can be determined considering that the solid carbon can be formed by the three reactions of carbon decomposition (R1), CO reduction (R2) and the Boudouard reaction (R3) [25,26]. On the CDB curve, the net amount of solid carbon production and consumption by these reactions is zero [27].

$$CH_4 \overset{K_{p,CD}}{\longleftrightarrow} C + 2H_2 \tag{R1}$$

$$K_{p,CD}(T) = \frac{x_{H_2,CDB}^2 (p - p_{ig})}{x_{CH_4,CDB}} \tag{5}$$

$$H_2 + CO \overset{K_{p,COR}}{\longleftrightarrow} C + H_2O \tag{R2}$$

$$K_{p,COR}(T) = \frac{x_{H_2O,CDB}}{x_{H_2,CDB} x_{CO,CDB} (p - p_{ig})} \tag{6}$$

$$2CO \overset{K_{p,B}}{\longleftrightarrow} C + CO_2 \tag{R3}$$

$$K_{p,B}(T) = \frac{x_{CO_2,CDB}}{x_{CO,CDB}^2 (p - p_{ig})} \tag{7}$$

The mole fractions of CH_4, H_2O and CO_2 at the given fuel temperature, total pressure, and partial pressure of the inert gases are

determined from Eqs. (5)–(7), as follows:

$$x_{CH_4,CDB} = \frac{x^2_{H_2,CDB}(p - p_{ig})}{K_{p,CD}(T)} \quad (8)$$

$$x_{H_2O,CDB} = K_{p,COR}(T)x_{H_2,CDB}x_{CO,CDB}(p - p_{ig}) \quad (9)$$

$$x_{CO_2,CDB} = K_{p,B}(T)x^2_{CO,CDB}(p - p_{ig}) \quad (10)$$

By substituting Eqs. (8)–(10) into Eq. (1), the mole fraction of H_2 can be determined as a function of the mole fraction of CO.

$$x_{H_2,CDB} = 0.5K_{p,CD}(T)\left(\frac{1}{(p - p_{ig})} + K_{p,COR}(T)x_{CO,CDB}\right) \times \left(\sqrt{1 + \frac{4\left(\frac{1-x_{CO,CDB}}{(p-p_{ig})} - K_{p,B}(T)x^2_{CO,CDB}\right)}{K_{p,CD}(T)\left(\frac{1}{(p-p_{ig})} + K_{p,COR}(T)x_{CO,CDB}\right)^2}} - 1\right) \quad (11)$$

The composition of fuels that makes the CDB curve in the C–H–O ternary diagram is determined using Eqs. (8)–(11) by changing the mole fraction of carbon monoxide from 0 to $x_{CO,CDB,max}$.

$$0 \le x_{CO,CDB} \le x_{CO,CDB,max} = \frac{\sqrt{1 + 4K_{p,B}(T)(p - p_{ig})} - 1}{2K_{p,B}(T)(p - p_{ig})} \quad (12)$$

2.2. Maximum cell voltage

To obtain the MCV of SOFCs, it is assumed that the fuel utilization ratio is sufficiently high so that the minimum local Nernst voltage and the maximum local internal resistance in a cell take place at the end of the anode. From the Nernst voltage equation:

$$MCV = \frac{-R_u T_o}{2F}(\alpha + \ln(\varepsilon)) \quad (13)$$

$$\alpha = \frac{\bar{g}^0_{H_2O}(T_o) - \bar{g}^0_{H_2}(T_o) - 0.5\bar{g}^0_{O_2}(T_o)}{R_u T_o} - 0.5\ln(x_{O_2}p) \quad (14)$$

$$\varepsilon = \frac{x_{H_2O,o}}{x_{H_2,o}} \quad (15)$$

To determine the MCV, Eq. (15) should be expanded. For this purpose, the molar flow rate of each species in the outlet fuel is derived as follows:

$$\dot{n}_{CH_4,o} = \dot{n}_{CH_4,i} - \dot{C}_{CH_4} \quad (16)$$

$$\dot{n}_{CO_2,o} = \dot{n}_{CO_2,i} + \dot{P}_{CO_2} \quad (17)$$

$$\dot{n}_{CO,o} = \dot{n}_{CO,i} + \dot{C}_{CH_4} - \dot{P}_{CO_2} \quad (18)$$

$$\dot{n}_{H_2,o} = \dot{n}_{H_2,i} + 3\dot{C}_{CH_4} + \dot{P}_{CO_2} - \dot{C}_{H_2} \quad (19)$$

$$\dot{n}_{H_2O,o} = \dot{n}_{H_2O,i} - \dot{C}_{CH_4} - \dot{P}_{CO_2} + \dot{C}_{H_2} \quad (20)$$

$$\dot{n}_{ig,o} = \dot{n}_{ig,i} \quad (21)$$

$$U_f = \frac{\begin{array}{c}[(\dot{n}_{H_2,i} - \dot{n}_{H_2,o})(\bar{h}_{H_2O}(T_i) - \bar{h}_{H_2}(T_i) - 0.5\bar{h}_{O_2}(T_i)) + (\dot{n}_{CO,i} - \dot{n}_{CO,o})(\bar{h}_{CO_2}(T_i) - \bar{h}_{CO}(T_i) - 0.5\bar{h}_{O_2}(T_i)) \\ + (\dot{n}_{CH_4,i} - \dot{n}_{CH_4,o})(\bar{h}_{CO_2}(T_i) + 2\bar{h}_{H_2O}(T_i) - \bar{h}_{CH_4}(T_i) - 2\bar{h}_{O_2}(T_i))]\end{array}}{\begin{array}{c}[\dot{n}_{H_2,i}(\bar{h}_{H_2O}(T_i) - \bar{h}_{H_2}(T_i) - 0.5\bar{h}_{O_2}(T_i)) + \dot{n}_{CO,i}(\bar{h}_{CO_2}(T_i) - \bar{h}_{CO}(T_i) - 0.5\bar{h}_{O_2}(T_i)) \\ + \dot{n}_{CH_4,i}(\bar{h}_{CO_2}(T_i) + 2\bar{h}_{H_2O}(T_i) - \bar{h}_{CH_4}(T_i) - 2\bar{h}_{O_2}(T_i))]\end{array}} \quad (32)$$

where $\dot{C}_{H_2}$ and $\dot{C}_{CH_4}$ are, respectively, the rates of the hydrogen and methane consumption by reactions (R4) and (R5) and $\dot{P}_{CO_2}$ is the rate of the carbon dioxide production by reaction (R6).

$$H_2 + O^{2-} \rightarrow H_2O + 2e^- \quad (R4)$$

$$CH_4 + H_2O \overset{K_{p,SR}}{\longleftrightarrow} CO + 3H_2 \quad (R5)$$

$$K_{p,SR}(T) = \frac{x_{CO}x^3_{H_2}(p - p_{ig})^2}{x_{CH_4}x_{H_2O}} \quad (22)$$

$$CO + H_2O \overset{K_{p,WGS}}{\longleftrightarrow} CO_2 + H_2 \quad (R6)$$

$$K_{p,WGS}(T) = \frac{x_{CO_2}x_{H_2}}{x_{CO}x_{H_2O}} \quad (23)$$

The difference of the molar flow rate of the outlet fuel and the inert gases is obtained from Eqs. (16)–(20) as follows:

$$(\dot{n}_o - \dot{n}_{ig,o}) = (\dot{n}_i - \dot{n}_{ig,i}) + 2\dot{C}_{CH_4} \quad (24)$$

By dividing Eqs. (16)–(20) by Eq. (24), the mole fractions of CH_4, CO_2, CO, H_2, and H_2O in the outlet fuel are obtained.

$$x_{CH_4,o} = \frac{x_{CH_4,i} - \dot{C}_{CH_4}/(\dot{n}_i - \dot{n}_{ig,i})}{1 + 2\dot{C}_{CH_4}/(\dot{n}_i - \dot{n}_{ig,i})} \quad (25)$$

$$x_{CO_2,o} = \frac{x_{CO_2,i} + \dot{P}_{CO_2}/(\dot{n}_i - \dot{n}_{ig,i})}{1 + 2\dot{C}_{CH_4}/(\dot{n}_i - \dot{n}_{ig,i})} \quad (26)$$

$$x_{CO,o} = \frac{x_{CO,i} + \dot{C}_{CH_4}/(\dot{n}_i - \dot{n}_{ig,i}) - \dot{P}_{CO_2}/(\dot{n}_i - \dot{n}_{ig,i})}{1 + 2\dot{C}_{CH_4}/(\dot{n}_i - \dot{n}_{ig,i})} \quad (27)$$

$$x_{H_2,o} = \frac{x_{H_2,i} + 3\dot{C}_{CH_4}/(\dot{n}_i - \dot{n}_{ig,i}) + \dot{P}_{CO_2}/(\dot{n}_i - \dot{n}_{ig,i}) - \dot{C}_{H_2}/(\dot{n}_i - \dot{n}_{ig,i})}{1 + 2\dot{C}_{CH_4}/(\dot{n}_i - \dot{n}_{ig,i})} \quad (28)$$

$$x_{H_2O,o} = \frac{x_{H_2O,i} - \dot{C}_{CH_4}/(\dot{n}_i - \dot{n}_{ig,i}) - \dot{P}_{CO_2}/(\dot{n}_i - \dot{n}_{ig,i}) + \dot{C}_{H_2}/(\dot{n}_i - \dot{n}_{ig,i})}{1 + 2\dot{C}_{CH_4}/(\dot{n}_i - \dot{n}_{ig,i})} \quad (29)$$

By substituting Eqs. (28) and (29) into Eq. (15), this equation is expanded as follows:

$$\varepsilon = \frac{x_{H_2O,i} - \dot{C}_{CH_4}/(\dot{n}_i - \dot{n}_{ig,i}) - \dot{P}_{CO_2}/(\dot{n}_i - \dot{n}_{ig,i}) + \dot{C}_{H_2}/(\dot{n}_i - \dot{n}_{ig,i})}{x_{H_2,i} + 3\dot{C}_{CH_4}/(\dot{n}_i - \dot{n}_{ig,i}) + \dot{P}_{CO_2}/(\dot{n}_i - \dot{n}_{ig,i}) - \dot{C}_{H_2}/(\dot{n}_i - \dot{n}_{ig,i})} \quad (30)$$

The next step is to derive, $\dot{C}_{CH_4}/(\dot{n}_i - \dot{n}_{ig,i})$, $\dot{C}_{H_2}/(\dot{n}_i - \dot{n}_{ig,i})$ and $\dot{P}_{CO_2}/(\dot{n}_i - \dot{n}_{ig,i})$.

By utilizing the hydrogen along the anode and increasing the temperature of fuel, reaction (R5) is shifted to the right-side to consume almost all methane content of the outlet fuel from the anode; thus, from Eq. (25):

$$\frac{\dot{C}_{CH_4}}{\dot{n}_i - \dot{n}_{ig,i}} = x_{CH_4,i} \quad (31)$$

$\dot{C}_{H_2}/(\dot{n}_i - \dot{n}_{ig,i})$ can be obtained from the fuel utilization ratio equation, Eq. (32) [28–30], as Eq. (33).

$$\frac{\dot{C}_{H_2}}{(\dot{n}_i - \dot{n}_{ig,i})} = U_f\left(x_{H_2,i} + \frac{\gamma}{\beta}x_{CO,i} + \frac{\delta}{\beta}x_{CH_4,i}\right) - \left(\frac{\delta - \gamma}{\beta} - 3\right)x_{CH_4,i} - \left(\frac{\gamma}{\beta} - 1\right)\frac{\dot{P}_{CO_2}}{(\dot{n}_i - \dot{n}_{ig,i})} \quad (33)$$

where,

$$\beta = \frac{\bar{h}_{H_2O}(T_i) - \bar{h}_{H_2}(T_i) - 0.5\bar{h}_{O_2}(T_i)}{R_u T_o} \quad (34)$$

$$\gamma = \frac{\bar{h}_{CO_2}(T_i) - \bar{h}_{CO}(T_i) - 0.5\bar{h}_{O_2}(T_i)}{R_u T_o} \quad (35)$$

$$\delta = \frac{\bar{h}_{CO_2}(T_i) + 2\bar{h}_{H_2O}(T_i) - \bar{h}_{CH_4}(T_i) - 2\bar{h}_{O_2}(T_i)}{R_u T_o} \quad (36)$$

To obtain $\dot{P}_{CO_2}/(\dot{n}_i - \dot{n}_{ig,i})$, Eq. (23) is developed for the outlet fuel from the anode. Depending on the equilibrium constant of the water gas shift reaction at the temperature of the outlet fuel, $\dot{P}_{CO_2}/(\dot{n}_i - \dot{n}_{ig,i})$ is determined from the following equation:

$$\frac{\dot{P}_{CO_2}}{(\dot{n}_i - \dot{n}_{ig,i})} = -\left[(x_{CO,i} + x_{CH_4,i})\left(x_{CH_4,i}\left(\frac{\delta-\gamma}{\beta} - 2\right) - x_{H_2O,i} - U_f\left(x_{H_2,i} + \frac{\gamma}{\beta}x_{CO,i} + \frac{\delta}{\beta}x_{CH_4,i}\right)\right)\right.$$
$$\left. + x_{CO_2,i}\left(x_{H_2,i} + x_{CH_4,i}\left(\frac{\delta-\gamma}{\beta}\right) - U_f\left(x_{H_2,i} + \frac{\gamma}{\beta}x_{CO,i} + \frac{\delta}{\beta}x_{CH_4,i}\right)\right)\right] \Big/ \left[2x_{CH_4,i} + \left(\frac{\gamma}{\beta} - 1\right)\right.$$
$$\left. \times (x_{CO_2,i} + x_{CO,i} + x_{CH_4,i}) + 1\right] \qquad (K_{p,WGS}(T_o) = 1) \quad (37)$$

$$\frac{\dot{P}_{CO_2}}{(\dot{n}_i - \dot{n}_{ig,i})} = -\frac{\psi}{2} - \sqrt{\left(\frac{\psi}{2}\right)^2 - \omega} \qquad (K_{p,WGS}(T_o) > 1)$$

$$\frac{\dot{P}_{CO_2}}{(\dot{n}_i - \dot{n}_{ig,i})} = -\frac{\psi}{2} + \sqrt{\left(\frac{\psi}{2}\right)^2 - \omega} \qquad (K_{p,WGS}(T_o) < 1)$$

where,

$$\psi = \frac{\beta}{\gamma}\left[x_{H_2,i} + x_{CO_2,i} + x_{CH_4,i} - U_f\left(x_{H_2,i} + \frac{\gamma}{\beta}x_{CO,i} + \frac{\delta}{\beta}x_{CH_4,i}\right) + \left(\frac{\delta-\gamma}{\beta} - 3\right)x_{CH_4,i}\right.$$
$$\left. + \frac{2x_{CH_4,i} + \left(\frac{\gamma}{\beta} - 1\right)x_{CO_2,i} + K_{p,WGS}(T_o)\left(1 + \left(\frac{\gamma}{\beta} - 1\right)(x_{CO,i} + x_{CH_4,i})\right)}{1 - K_{p,WGS}(T_o)}\right] \quad (38)$$

$$\omega = \frac{\beta}{\gamma(1 - K_{p,WGS}(T_o))}\left[K_{p,WGS}(T_o)(x_{CO,i} + x_{CH_4,i})\left(x_{CH_4,i}\left(\frac{\delta-\gamma}{\beta} - 2\right) - x_{H_2O,i} - U_f\left(x_{H_2,i} + \frac{\gamma}{\beta}x_{CO,i} + \frac{\delta}{\beta}x_{CH_4,i}\right)\right)\right.$$
$$\left. + x_{CO_2,i}\left(x_{H_2,i} + x_{CH_4,i}\left(\frac{\delta-\gamma}{\beta}\right) - U_f\left(x_{H_2,i} + \frac{\gamma}{\beta}x_{CO,i} + \frac{\delta}{\beta}x_{CH_4,i}\right)\right)\right] \quad (39)$$

Therefore, at a given operating condition of anode inlet and outlet fuel temperatures; cell operating pressure; oxygen mole fraction at the cathode; and fuel utilization ratio, the MCV depends only on the anode inlet fuel composition.

2.3. Developing fuel map

In this step, the equations required to find the inlet fuels to the anode that yield identical MCV at the given operating condition are determined.

At a given operating condition and a specific MCV, the mole fraction of H_2O in the inlet fuel can be found from Eq. (13):

$$x_{H_2O,i} = \left(x_{H_2,i} + 3x_{CH_4,i} + \frac{\dot{P}_{CO_2}}{\dot{n}_i - \dot{n}_{ig,i}} - \frac{\dot{C}_{H_2}}{\dot{n}_i - \dot{n}_{ig,i}}\right) \times \left(\exp\left(\frac{-R_u T_o}{2F\,MCV} - \alpha\right) + 1\right) - x_{H_2,i} - 2x_{CH_4,i} \quad (40)$$

By solving Eqs. (1), (22) and (23) for the inlet fuel to the anode, the mole fraction of CO_2, CO, and CH_4 are determined as follows:

$$x_{CO_2,i} = \frac{K_{p,WGS}(T_i)x_{H_2O,i}^2(1 - x_{H_2O,i} - x_{H_2,i})}{K_{p,WGS}(T_i)x_{H_2O,i}^2 + x_{H_2,i}x_{H_2O,i} + \frac{x_{H_2,i}^4(p-p_{ig})^2}{K_{p,SR}(T_i)}} \quad (41)$$

$$x_{CO,i} = \frac{x_{H_2,i}x_{H_2O,i}(1 - x_{H_2O,i} - x_{H_2,i})}{K_{p,WGS}(T_i)x_{H_2O,i}^2 + x_{H_2}x_{H_2O,i} + (x_{H_2,i}^4(p-p_{ig})^2/K_{p,SR}(T_i))} \quad (42)$$

$$x_{CH_4,i} = \frac{x_{H_2,i}^4(p-p_{ig})^2/K_{p,SR}(T_i)(1 - x_{H_2O,i} - x_{H_2,i})}{K_{p,WGS}(T_i)x_{H_2O,i}^2 + x_{H_2,i}x_{H_2O,i} + (x_{H_2,i}^4(p-p_{ig})^2/K_{p,SR}(T_i))} \quad (43)$$

By changing the mole fraction of H_2 in the inlet fuel from 0 to 1, the compositions of the inlet fuels that yield an identical MCV for SOFCs at the given operating condition are determined from Eqs. (40)–(43). Among these fuels, those located below the CDB curve in the C–H–O ternary diagram are acceptable. These fuels create a continuous curve in the ternary coordinate system. A fuel map is established by developing the continuous fuel curves for different MCVs at the same operating condition and representing them in the C–H–O ternary diagram.

3. Results and discussion

The locations of some typical fuels, presented in Tables 1 and 2, are shown in Fig. 1. Most of these fuels are above the carbon deposition curve in the C–H–O ternary diagram (in the indirect fuel utilization region) and cannot be directly utilized in SOFC. Indeed, they should be transferred to below the CDB curve by combining them with a mixture (or a substance) located below the CDB curve

Table 1
A typical composition of some gaseous fuels.

Compound	mol%					
	NG[a] [31]	ADG[b] [32]	SRM[c] [33]	POM[d] [34]	FBCG[e] [35]	BPG[f] [36]
CH_4	88.5	60.8	2.4	1.0	4.6	4
C_2H_6	4.8	–	–	–	–	–
C_3H_8	1.6	–	–	–	–	–
C_4H_{10}	0.7	–	–	–	–	–
H_2	–	–	52.9	35.8	28.0	17
CO	–	–	0.50	18.9	33.0	13
H_2O	–	0.01	30.4	3.7	16.8	15
CO_2	–	34.8	13.0	0.8	15.0	11
N_2	4.4	2.4	0.8	39.8	0.6	40
O_2	–	1.5	–	–	–	–

[a] Natural gas.
[b] Anaerobic digestion gas.
[c] Gas produced by the steam reforming of methane.
[d] Gas produced by the partial oxidation of methane.
[e] Gas produced by the fluidized bed coal gasifier.
[f] Biomass produced gas.

(e.g. with steam for the case of the steam reforming or with oxygen for the case of the partial oxidation fuel processors). In the C–H–O ternary diagram, any possible combination of two different mixtures (or substances) lies on a line that connects the location of these two mixtures. Depending on the location of the new mixture on this line, the volumetric mixing ratio of mixture 2 to mixture 1 is obtained from Eq. (44).

$$y_{2/1} = z_{1/2}\left(\frac{C_1 - C_{1,2}}{C_{1,2} - C_2}\right) \tag{44}$$

where $z_{1/2}$ is the ratio of the number of atoms in mixture 1 to mixture 2, and $C_{1,2}$ is the carbon atom ratio of the new mixture. Hence, the volumetric mixing ratio of a fuel located above the CDB curve and a mixture (or a substance) below this curve, which makes a fuel that can be utilized in the anode, can be determined from Eq. (44).

3.1. Carbon deposition boundary

In Fig. 2, the effect of the fuel temperature and pressure on the CDB curve is shown. According to Fig. 2a, increasing the temper-

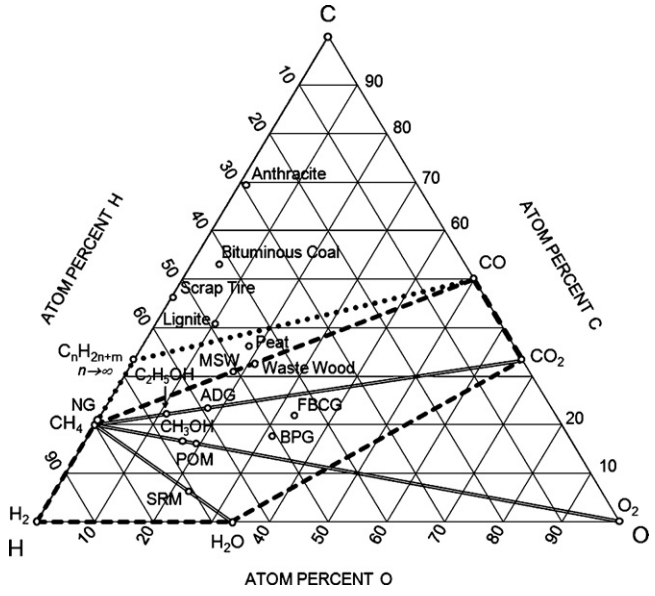

Fig. 1. The location of some fuels in the C–H–O ternary diagram.

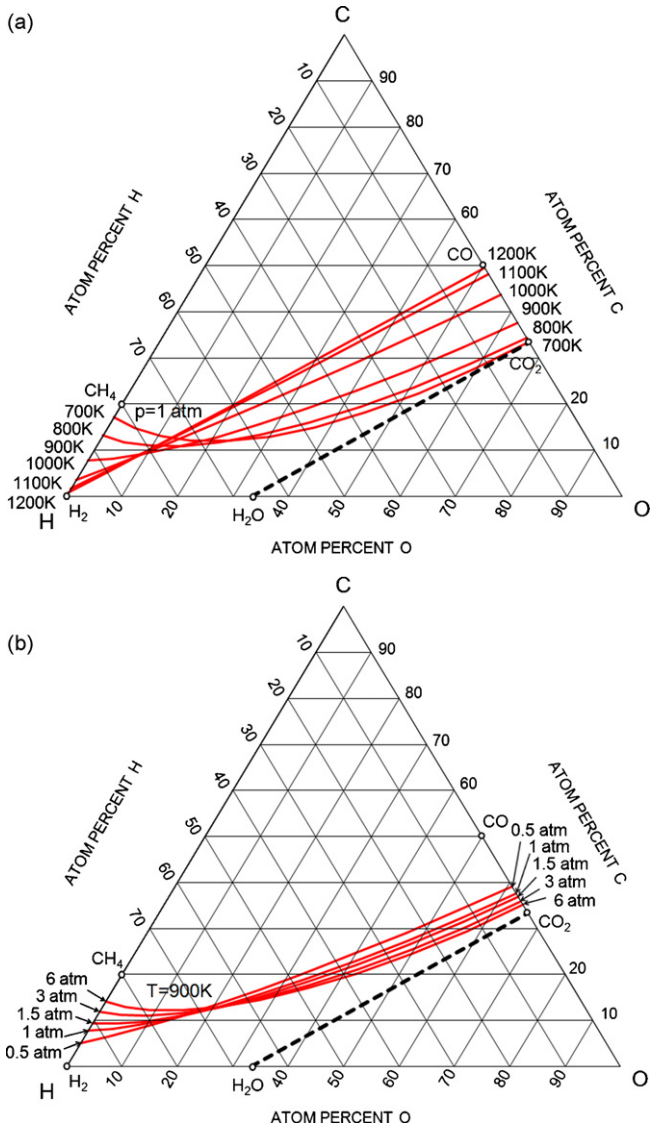

Fig. 2. The CDB curve in the C–H–O ternary diagram: (a) effect of temperature and (b) effect of pressure.

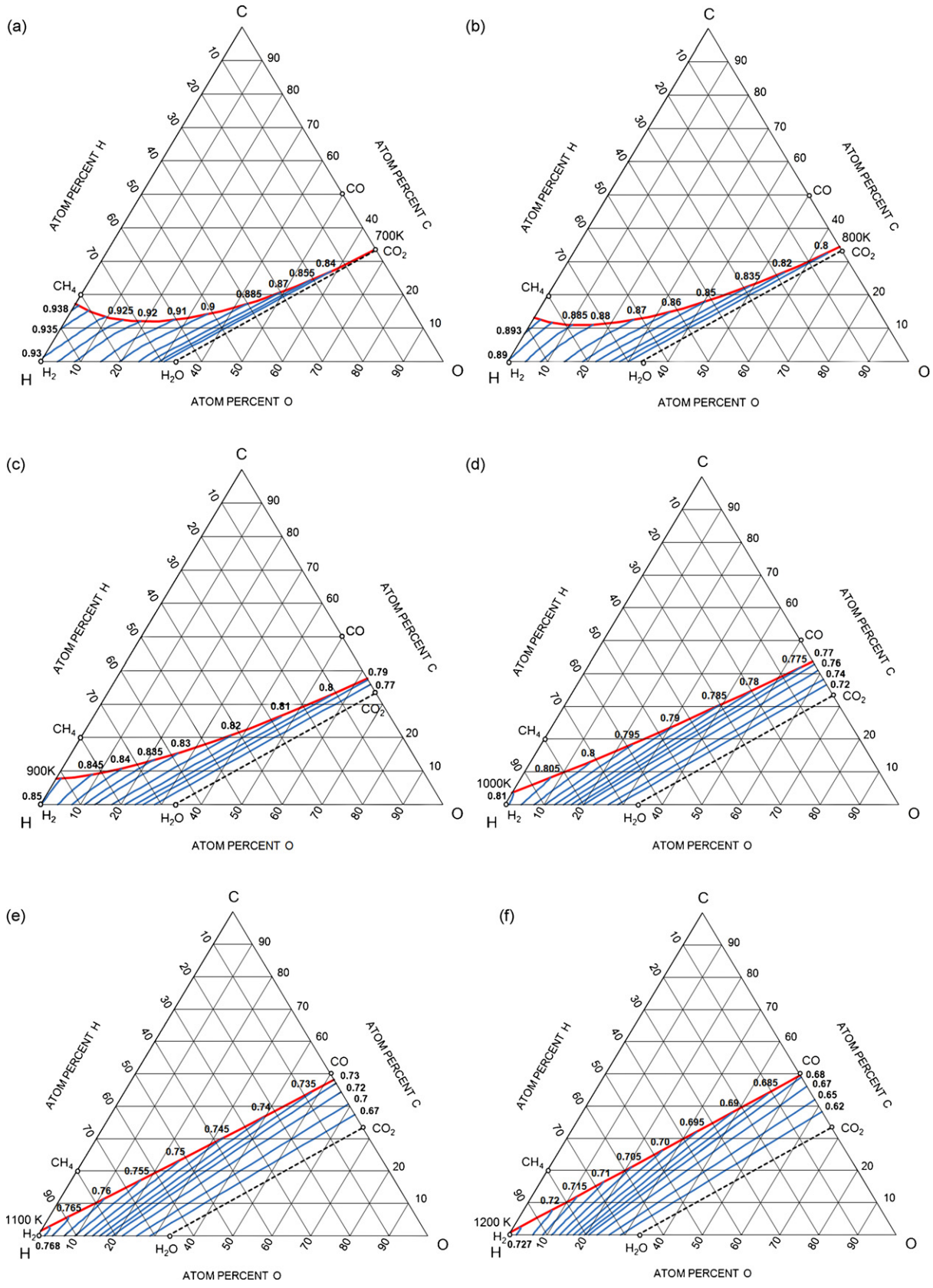

Fig. 3. Fuel map for the MCV of SOFCs operating at $p = 1$ atm, $U_f = 0.85$, $\Delta T = 200$ K, $x_{O_2} = 0.21$, $p_{ig} = 0$ and (a) $T_i = 700$ K, (b) $T_i = 800$ K, (c) $T_i = 900$ K, (d) $T_i = 1000$ K, (e) $T_i = 1100$ K, and (f) $T_i = 1200$ K.

Table 2
A typical composition of some solid fuels [37].

Feedstock	wt% (dry)					
	C	H	O	N	S	Ash
MSW[a]	37.7	5.1	30.1	1.2	0.1	25.8
Waste wood	41.6	4.9	36.2	0.3	0.01	17
Scrap tire	71.5	6.9	0.7	0.6	1	19.3
Peat	50.7	5.3	34.7	1.3	1.3	6.7
Lignite	60	6	20	2	2	10
Bituminous coal	73.9	4.9	9.2	1.4	0.8	9.8
Anthracite	89.5	3.1	2.1	1.1	1.1	3.1

[a] MSW: municipal solid waste.

Table 3
The fuels that yield the MCV = 0.82 V at T_i = 900 K, ΔT = 200 K, p = 1 atm, U_f = 0.85, and $x_{O_2} = 0.21$.

Fuel	mol%				
	x_{CH_4}	x_{H_2}	x_{CO}	x_{H_2O}	x_{CO_2}
1	0	56.8	0	43.2	0
2	0.5	54.3	1.6	40.8	2.8
3	0.9	52	3.3	38.2	5.6
4	1.4	49.5	5.1	35.6	8.4
5	1.7	47.0	7.0	33.0	11.3
6	2.0	44.5	9.0	30.4	14.1
7	2.3	42.0	11.1	27.8	16.8
8	2.7	36.9	15.6	22.7	22.1
9	2.8	34.2	18.2	20.2	24.6
10	2.9	31.5	20.8	17.8	27.0

ature causes the direct fuel utilization region to enlarge on the right- and shrink on the left-side of the C–H–O ternary diagram. At temperatures of more than 1200 K, the CDB curve is almost a straight line joining the points H_2 and CO together.

As shown in Fig. 2b, the effect of decreasing the pressure on the CDB curve is similar to the effect of reducing temperature. In fact, by increasing the pressure, the direct fuel utilization region shrinks on the right- and enlarges on the left-side. Based on Eqs. (8)–(11), the effect of inert gases on the CDB curve is equivalent to decreasing the total pressure of the gaseous fuel. This means that a gaseous fuel containing 20 mol% of inert gases is equivalent to the same fuel without any inert gas and a total pressure of 20% less than the fuel with inert gas.

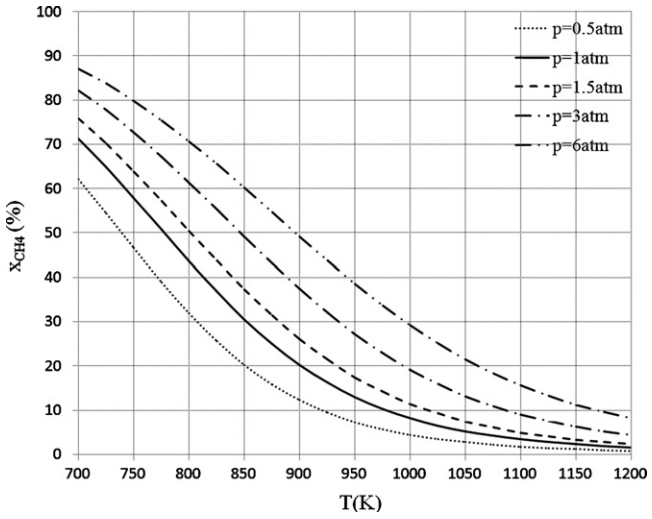

Fig. 4. Effect of the temperature on the mole fraction of methane in the fuel that yields the highest MCV for SOFCs at different cell operating pressures.

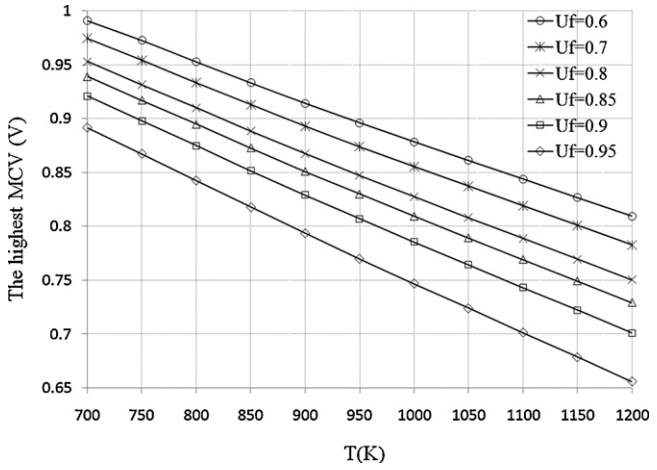

Fig. 5. Effect of the inlet fuel temperature on the highest MCV at different fuel utilization ratios (p = 1 atm, ΔT = 200 K, $x_{O_2} = 0.21$).

3.2. Maximum cell voltage

The predictions obtained from the current model for some fuels that yield the same MCV are shown in Table 3 for the inlet and outlet fuel temperatures of T_i = 900 K and T_o = 1100 K, respectively ($\Delta T = T_o - T_i$ = 200 K); the cell operating pressure of p = 1 atm; the fuel utilization ratio of U_f = 0.85; and the oxygen mole fraction of $x_{O_2} = 0.21$. According to this table, the presence of methane in the inlet fuel does not necessarily lead to an increase in the MCV.

In Fig. 3, the fuel maps to predict the effect of fuel composition on the MCV are shown for different inlet fuel temperatures of 700 K, 800 K, 900 K, 1000 K, 1100 K, and 1200 K at p = 1 atm, U_f = 0.85, ΔT = 200 K, $x_{O_2} = 0.21$, and p_{ig} = 0. It can be seen from this figure the

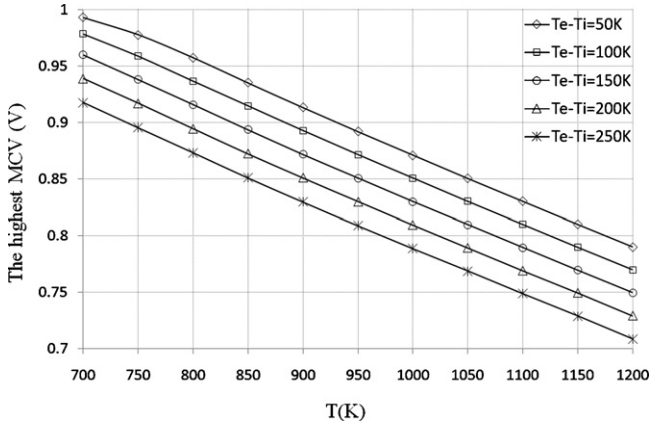

Fig. 6. Effect of the inlet fuel temperature on the highest MCV at different fuel temperature rises along the anode (p = 1 atm, U_f = 0.85, $x_{O_2} = 0.21$).

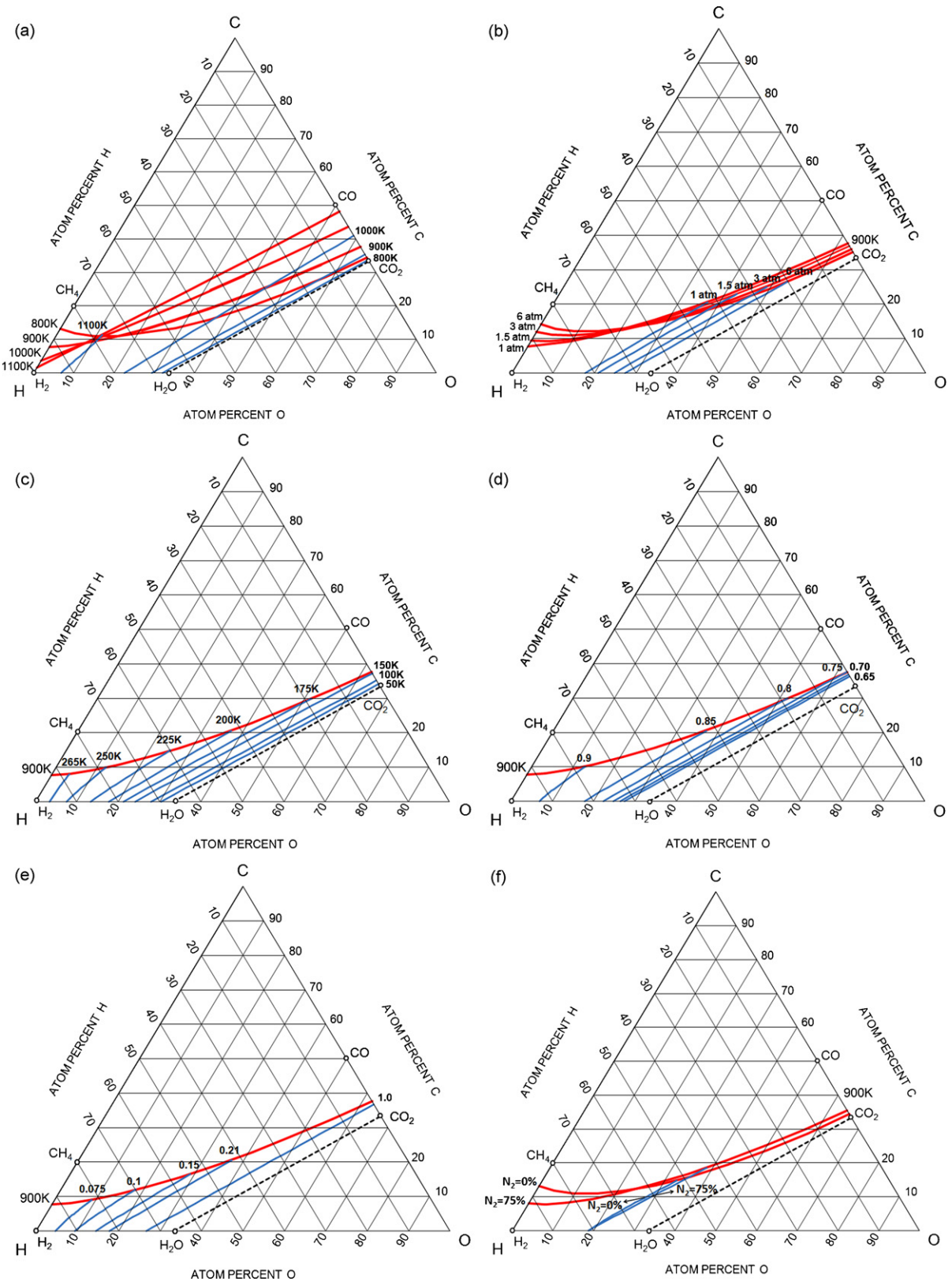

Fig. 7. Effect of the (a) temperature of the inlet fuel to the anode at MCV = 0.76 V, p = 1 atm, U_f = 0.85, ΔT = 200 K, $x_{O_2} = 0.21$, p_{ig} = 0, (b) cell operating pressure at MCV = 0.82 V, T_i = 900 K, U_f = 0.85, ΔT = 200 K, $x_{O_2} = 0.21$, p_{ig} = 0, (c) fuel temperature rise along the anode at MCV = 0.82 V, T_i = 900 K, p = 1 atm, U_f = 0.85, $x_{O_2} = 0.21$, p_{ig} = 0, (d) fuel utilization ratio at MCV = 0.82 V, T_i = 900 K, p = 1 atm, ΔT = 200 K, $x_{O_2} = 0.21$, p_{ig} = 0, (e) oxygen mole fraction in cathode at MCV = 0.82 V, T_i = 900 K, p = 1 atm, U_f = 0.85, ΔT = 200 K, p_{ig} = 0, and (f) nitrogen mole fraction (as an inert gas) at MCV = 0.86 V, T_i = 800 K, p = 1 atm, U_f = 0.85, ΔT = 200 K, $x_{O_2} = 0.21$, on the continuous fuel curves.

type of fuel has a significant effect on the MCV. The following general results can be obtained for the fuels in the direct and indirect fuel utilization regions in the C–H–O ternary diagram.

3.2.1. Direct fuel utilization region

Among the fuels with the same percentage of carbon atom, the one with a higher percentage of hydrogen atom yields a higher MCV at a given operating condition. If the location of a fuel is either below or at right of another fuel in the C–H–O ternary diagram, it yields a lower MCV.

Among the fuels that are at the same temperature and pressure, the highest MCV is yielded by the one located at the intersection of the CDB curve and the H–C axis in the C–H–O ternary diagram. This fuel contains only H_2 and CH_4; however, a small quantity of water should be added to start the electrochemical reaction in anode. For this fuel, the mole fraction of CH_4 as a function of the inlet fuel temperature at different cell operating pressures is shown in Fig. 4. It is observed that decreasing the inlet fuel temperature and increasing the cell operating pressure leads to an increase in the mole fraction of CH_4. At inlet fuel temperatures of more than 1200 K and a cell operating pressure of the order of 1 atm, almost pure hydrogen is the fuel that yields the highest MCV for SOFCs. The effect of the inlet fuel temperature on the highest MCV at different fuel utilization ratios and fuel temperature rises along the anode ($T_o - T_i$) are illustrated in Figs. 5 and 6, respectively. According to these figures, for each 100 K increase in the inlet fuel temperature, the highest MCV reduces around 0.04 V. Increasing the fuel utilization ratio and fuel temperature rise along the anode causes a decrease in the highest MCV.

In many cases, for a fuel in the direct fuel utilization region, the MCV can be increased by mixing it with a fuel which is in the indirect fuel utilization region. For example, if a mixture of 85 mol% biomass produced gas (BPG) and 15 mol% natural gas (NG), see Fig. 1, is utilized in an SOFC instead of utilizing only the BPG, based on the fuel map presented in Fig. 3e, the MCV increases from 0.73 V to 0.75 V at the operating condition of T_i = 1100 K, p = 1 atm, U_f = 0.85, ΔT = 200 K, and $x_{O_2} = 0.21$.

3.2.2. Indirect fuel utilization region

In the indirect fuel utilization region, the fuel composition and the type of the fuel processor affects the MCV of SOFCs. Among the fuels with the same percentage of carbon atom, a fuel with a higher percentage of hydrogen atom yields a higher MCV at a given operating condition, regardless of the type of the fuel processor.

We decided to use an example to explain the effect of different types of fuel processors on MCV. In this example, CH_4 at a temperature of 900 K is considered as the inlet fuel to the anode. Using Fig. 2a, we can determine that this fuel is in the indirect fuel utilization region and should be processed before it can be utilized in the anode. If partial oxidation is selected as a fuel processor, according to Eq. (44) and Fig. 3c, at least 0.86 moles of O_2 should be added to each mole of CH_4 to cross the CDB curve which will then result in an MCV value around 0.83 V. If steam reforming is selected as the fuel processor, at least 1.4 moles of H_2O should be added to each mole of CH_4 and the MCV will be around 0.84 V. For the auto-thermal reforming fuel processor, depending on how much H_2O and O_2 are added to CH_4, the MCV varies from 0.83 V to 0.84 V. The dry reforming of CH_4 at 900 K is possible by adding almost 6.7 moles of CO_2 to each mole of CH_4; however, the MCV reaches around 0.8 V. If four moles of H_2 are added to each mole of CH_4 at 900 K, the MCV corresponding to the new mixture will be around 0.85 V. The effect of the anode exit gas recirculation on the MCV is the same as the partial oxidation with oxygen. As a general result, for any fuel in the indirect fuel utilization region, the steam reforming fuel processor yields a higher MCV than the partial oxidation and auto-thermal reforming fuel processors at a specific operating condition.

3.3. Effect of the operating condition

To predict the effect of the operating condition of a cell on the location of the continuous fuel curves in fuel maps, a parametric study is performed and the results are shown in Fig. 7. According to Fig. 7a, decreasing the temperature of the inlet fuel to the anode shifts the continuous fuel curves to the right of the fuel map. This means that fuels with a lower hydrogen atom percentage (with the same percentage of carbon atom) can still yield a high MCV if the inlet fuel temperature is reduced. Based on Fig. 7b, by decreasing the cell operating pressure, the continuous fuel curves tend to move to the left. As observed in Fig. 7c and d, by decreasing the fuel temperature rise along the anode and the fuel utilization ratio, the continuous fuel curves shift to the right of the fuel map. By decreasing the oxygen mole fraction in cathode, the continuous fuel curves shift to the left of the fuel map (Fig. 7e). According to Fig. 7f, there is no significant change in the location of continuous fuel curves between a fuel without any inert gas and a fuel with 75 mol% inert gas.

4. Conclusions

At any operating condition, a fuel map can be developed for SOFCs to predict the effect of the composition of any fuel containing carbon, hydrogen, oxygen, and inert gas atoms on the MCV. The fuel maps are also useful for selecting an appropriate fuel processor for the fuels that cannot be directly utilized in SOFCs due to the carbon deposition problem. Some of the general results obtained in this study are as follows:

- The composition of a fuel has a significant effect on the MCV of SOFCs.
- Among fuels with the same percentage of carbon atom, a fuel with a higher percentage of hydrogen atom yields a higher MCV at a given operating condition.
- In the direct fuel utilization region, if the location of a fuel is either below or right-side of another fuel in the fuel map, it yields a lower MCV.
- Among the fuels in the direct fuel utilization region, at the same temperature and pressure, the highest MCV is always obtained from a fuel located at the intersection of the CDB curve and the H–C axis in the fuel map.
- In the indirect fuel utilization region, the composition of a fuel and the type of the fuel processor affect the MCV.
- For any fuel in the indirect fuel utilization region, the steam reforming fuel processor yields a higher MCV than the partial oxidation and auto-thermal reforming fuel processors at a given operating condition of a cell.
- Decreasing the cell operating pressure and the oxygen mole fraction (in cathode) shifts continuous fuel curves to the left of the fuel map.
- Decreasing the temperature of the inlet fuel to the anode; the fuel temperature rise along the anode; or the fuel utilization ratio, shifts the continuous fuel curves to the right of the fuel map.
- The partial pressure of inert gases does not have any significant effect on the location of continuous fuel curves.

Acknowledgement

The authors gratefully acknowledge financial supports provided by the Natural Sciences and Engineering Research Council of Canada (NSERC).

References

[1] L.E. Arteaga, L.M. Peralta, V. Kafarov, Y. Casas, E. Gonzales, Chem. Eng. J. 136 (2008) 256–266.

[2] R.J. Braun, S.A. Kleina, D.T. Reindla, J. Power Sources 158 (2) (2006) 1290–1305.
[3] S.H. Chan, O.L. Ding, Int. J. Hydrogen Energy 30 (2005) 167–179.
[4] P. Piroonlerkgul, S. Assabumrungrat, N. Laosiripojana, A.A. Adesina, Chem. Eng. J. 140 (2008) 341–351.
[5] N. Hotz, S.M. Senn, D. Poulikakos, J. Power Sources 158 (2006) 333–347.
[6] A. Franzoni, L. Magistri, A. Traverso, A.F. Massardo, Energy 33 (2008) 311–320.
[7] V. Modafferi, G. Panzera, V. Baglio, F. Frusteri, P.L. Antonucci, Appl. Catal. A: Gen. 334 (2008) 1–9.
[8] C.O. Colpan, I. Dincer, F. Hamdullahpur, Int. J. Hydrogen Energy 32 (2007) 787–795.
[9] R. Peters, E. Riensche, P. Cremer, J. Power Sources 86 (2000) 432–441.
[10] E.J. Cairns, A.D. Tevebaugh, J. Chem. Eng. Data 9 (3) (1964) 453–462.
[11] G.H.J. Broers, B.W. Treijte, Adv. Energy Conv. 5 (1965) 365–382.
[12] K. Sasaki, Y. Teraoka, J. Electrochem. Soc. 150 (7) (2003) A878–A884.
[13] D. Singh, E. Hernandez-Pacheco, P.N. Hutton, N. Patel, M.D. Mann, J. Power Sources 142 (2005) 194–199.
[14] A.L. Dicks, J. Power Sources 71 (1998) 111–122.
[15] V. Alderucci, P.L. Antonucci, G. Maggio, N. Giordano, V. Antonucci, Int. J. Hydrogen Energy 19 (4) (1994) 369–376.
[16] S. Assabumrungrat, N. Laosiripojana, V. Pavarajarn, W. Sangtongkitcharoen, A. Tangjitmatee, P. Praserthdam, J. Power Sources 139 (2005) 55–60.
[17] W. Sangtongkitcharoen, S. Assabumrungrat, V. Pavarajarn, N. Laosiripojana, P. Praserthdam, J. Power Sources 142 (2005) 75–80.
[18] J. Koh, B. Kang, C.H. Lim, Y. Yoo, Electrochem. Solid-State Lett. 4 (2) (2001) A12–A15.
[19] C.O. Colpan, I. Dincer, F. Hamdullahpur, Int. J. Energy Res. 32 (2008) 336–355.
[20] E.S. Hecht, G.K. Gupta, H. Zhu, A.M. Dean, R.J. Kee, L. Maier, O. Deutschmann, Appl. Catal. A: Gen. 295 (2005) 40–51.
[21] A. Sacco, F.W.A.H. Geurts, G.A. Jablonski, S. Lee, R.A. Gately, J. Catal. 119 (1989) 322–341.
[22] T. Takeguchi, Y. Kani, T. Yano, R. Kikuchi, K. Eguchi, K. Tsujimoto, Y. Uchida, A. Ueno, K. Omoshiki, M. Aizawa, J. Power Sources 112 (2002) 588–595.
[23] J. Macek, B. Novosel, M. Marinsek, J. Eur. Ceram. Soc. 27 (2007) 487–491.
[24] T. Horita, K. Yamaji, T. Kato, H. Kishimoto, Y. Xiong, N. Sakai, M.E. Brito, H. Yokokawa, J. Power Sources 145 (2005) 133–138.
[25] S. Chern, L.T. Fan, W.P. Walawender, AIChE J. 35 (4) (1989) 673–675.
[26] G.F. Froment, J. Mol. Catal.: Chem. 163 (2000) 147–156.
[27] K. Sasaki, Y. Teraoka, J. Electrochem. Soc. 150 (7) (2003) A885–A888.
[28] H. Zhu, R.J. Kee, J. Power Sources 161 (2006) 957–964.
[29] B. Thorstensen, J. Power Sources 92 (2001) 9–16.
[30] Y. Hao, D.G. Goodwin, J. Power Sources 183 (2008) 157–163.
[31] S. Farhad, M. Younessi-Sinaki, M.R. Golriz, F. Hamdullahpur, Int. J. Exergy 5 (2) (2008) 164–176.
[32] B.A. Peppley, Int. J. Green Energy 3 (2) (2006) 201–218.
[33] Fuel Cell Handbook, 7th ed., EG&G Technical Services, Inc., U.S. Department of Energy, 2004.
[34] M. Lyubovsky, H. Karim, P. Menacherry, S. Boorse, R. LaPierre, W.C. Pfefferle, S. Royudhury, Catal. Today 83 (2003) 183–197.
[35] T. Kivisaari, P. Björnbom, C. Sylwan, B. Jacquinot, D. Jansen, A. de Groot, Chem. Eng. J. 100 (2004) 167–180.
[36] A.O. Omosun, A. Bauen, N.P. Brandon, C.S. Adjiman, D. Hart, J. Power Sources 131 (2004) 96–106.
[37] J. Wochele, Paul Scherrer Institut (PSI), 2003.